Ore Geology Reviews 100 (2018) 168–182

Contents lists available at ScienceDirect

Ore Geology Reviews

journal homepage: www.elsevier.com/locate/oregeo

Chlorite and epidote chemistry of the Yandong Cu deposit, NW China: Metallogenic and exploration implications for Paleozoic porphyry Cu systems in the Eastern Tianshan

Bing Xiao [a,b], Huayong Chen [a,c,d,*], Yunfeng Wang [a], Jinsheng Han [a], Chao Xu [a], Juntao Yang [e]

[a] Key Laboratory of Mineralogy and Metallogeny, Guangzhou Institute of Geochemistry, Chinese Academy of Sciences, Guangzhou 510640, China
[b] Graduate University of Chinese Academy of Sciences, Beijing 100049, China
[c] State Key Laboratory of Ore Deposit Geochemistry, Institute of Geochemistry, Chinese Academy of Sciences, Guiyang 550002, China
[d] Guangdong Provincial Key Laboratory of Mineral Physics and Materials, Guangzhou 510640, China
[e] No. 1 Geological Party of the Xinjiang Bureau of Geology and Mineral Resources, Changji, 831100, China

ARTICLE INFO

Article history:
Received 25 October 2016
Received in revised form 2 March 2017
Accepted 3 March 2017
Available online 12 March 2017

Keywords:
Yandong Cu deposit
Chlorite and epidote geochemistry
Metallogeny
Eastern Tianshan
Central Asian Orogenic Belt

ABSTRACT

The Yandong porphyry Cu deposit in the Eastern Tianshan terrane is the largest in Xinjiang, NW China (metal reserve: 2.3 Mt Cu @ 0.67%). Three periods and six alteration and mineralization stages were identified in this study, i.e., Porphyry period (including Stage I: propylitic alteration; II: quartz-magnetite alteration; III: phyllic alteration and early mineralization); overprinting period (including Stage IV: overprinting mineralization and Stage V: late vein) and supergene period (Stage VI: supergene mineralization). Stage IV was the main Cu mineralization stage at the Yandong Cu deposit, which is characterized by the mineral assemblage of chalcopyrite + chlorite + anhydrite + calcite.

Electron microprobe analysis (EMPA) data indicate that Stage IV chlorite contains lower SiO_2 and MgO, but higher FeO, Al_2O_3 and Fe/(Fe + Mg) than Stage I chlorite. LA-ICP-MS analyses indicate that Stage IV chlorite contains lower Cr, Ni, Co, B, Ca and Sr, but higher Sc, Ga, Sn, Ti, Zn and Mn than Stage I chlorite. Stage IV epidote contains lower B, Zr, Ba and Ti, but higher Sn, Y, Ga, Ag, U, Y, Cu and Sr than Stage I epidote. Concentrations of Ti, Zn, As, V, Sc and Cu are highest near the orebody for both Stage I and IV chlorite, and Au and Sn in Stage IV chlorite are highest near the orebody. Titanium content of Stage I epidote is highest near the orebody, but V, Sc and Zr are lowest there. Stage I chlorite at Yandong is geochemically similar to the giant Batu Hijau porphyry Cu-Au deposit (Indonesia), but Stage IV chlorite contains higher Fe, Al and As, lower Mg and Sn than the latter. Stage I epidote at Yandong is geochemically similar to the porphyry and skarn deposits in the central Baguio district (Philippines), but Stage IV epidote has higher Sn, Ga and U, but lower Zr, Ti and Ba than the latter.

Ore deposit geology and alteration mineral chemistry indicate that the Yandong Cu deposit is an atypical porphyry deposit. The adakitic tonalite porphyry and quartz albite porphyry (granitic) may have formed the early and overprinting Cu mineralization, respectively. Chlorite Ti and V, and epidote Sb show similar spatial variation patterns in Cenozoic and Paleozoic porphyry deposits, which may be used for exploration targeting for ancient porphyry deposits, such as the Yandong Cu deposit.

1. Introduction

The gradual depletion of surficial or shallow-level mineral resources have driven mineral exploration towards deeper levels and decreasing grades (Cooke et al., 2014), and the development of a reliable exploration targeting tool to discover blind orebodies at depth has long been a challenge (Cameron et al., 2010; Carranza and Sadeghi, 2012). Recent research showed that trace element compositions of alteration minerals could provide vectoring information towards hydrothermal centers, and distinguish different types of chlorite from various hydrothermal systems. For example, LA-ICP-MS analyses of porphyry indicator minerals (such as chlorite, epidote and alunite) from Cenozoic porphyry systems revealed lateral and vertical trace element variations at different distances from the orebody, which can be used as proximity indicator to these young porphyry systems (Chang et al., 2011; Cooke et al.,

* Corresponding author at: Key Laboratory of Mineralogy and Metallogeny, Guangzhou Institute of Geochemistry, Chinese Academy of Sciences, Guangzhou 510640, China.
E-mail address: huayongchen@gig.ac.cn (H. Chen).

http://dx.doi.org/10.1016/j.oregeorev.2017.03.004
0169-1368/

2014; Wilkinson et al., 2015). Compared with the young porphyry systems, ancient mineralized porphyry systems have experienced more complex post-mineralization geological modifications, and whether such modifications would affect the geochemistry of these indicator minerals, and thus the reliability of the vectoring tool, is yet to be well-understood.

Chlorite and epidote are common alteration minerals in diverse geological settings and ore deposits (e.g., Cu, Au and U) (Sillitoe, 2010; Zhong et al., 2012; Jago et al., 2014; Dora and Randive, 2015; Wilkinson et al., 2015), and are thus useful in determining alteration processes, fluid compositions and physicochemical conditions of mineralization (Bryndzia and Scott, 1987; Zang and Fyfe, 1995; Zhong et al., 2012). Based on chlorite thermodynamic studies, Cathelineau (1988) found that the $Al_{(IV)}$ content in the tetrahedral site of chlorite increases with temperature. Arnason et al. (1993) concluded that temperature, along with O_2 and CO_2 fugacities, are the most important controls for local variations of epidote compositions.

The Central Asian Orogenic Belt (CAOB) is one of the world's most important porphyry copper belts, and hosts a number of giant / large Paleozoic porphyry copper deposits (Watanabe and Stein, 2000; Perelló et al., 2001; Xiao et al., 2009; Yang et al., 2012; Wu et al., 2015). Large porphyry copper deposits are rare in northern China, with the largest one being the Yandong Cu deposit in Xinjiang (NW China), which contains about 2.3 million tonnes (Mt) contained Cu @ 0.67% (No. 1 Brigade of the Xinjiang Bureau of Geology and Mineral Resources (#1XJBGMR), 2012). Since its discovery in the late 1990's, many studies were undertaken on its geology, age and geochemistry of the intrusions, mineralization age and ore-forming fluids (Han et al., 2006; Zhang et al., 2006, 2010; Shen et al., 2014a; Wang et al., 2015; Xiao et al., 2016). However, the hydrothermal alteration and mineralization of the Yandong Cu deposit remain controversial (Han et al., 2006; Zhang et al., 2010; Shen et al., 2014a; Xiao et al., 2016).

In this study, we present detailed ore deposit geological investigation and new EMPA and laser ablation inductively-coupled plasma mass spectrometry (LA-ICP-MS) analyses of the Yandong chlorite and epidote. We discuss the mineral trace element changes at different distances (lateral and vertical) from the Yandong orebodies and their genetic and exploration implications.

2. Regional geology

The Eastern Tianshan terrane between the Siberian and Tarim plates is an important component of CAOB, and ranks one of the most important metallogenic belts in NW China (Xiao et al., 2004; Chen et al., 2012). It comprises five tectonic units (from south to north): the Middle Tianshan massif, Aqishan-Yamansu belt, Kanggur shear zone, and the Dananhu-Tousuquan and Harlik magmatic arcs, bounded by a series of EW-trending faults including the Aqikekuduke, Yamansu, Kanggur and Dacaotan faults (Fig. 1A).

The Middle Tianshan massif contains mainly Devonian to Carboniferous calc-alkaline basaltic to andesitic volcanic and volcaniclastic rocks, and minor I-type granodiorites and granites and Precambrian basement rocks. The massif contains many Pb-Zn deposits, such as Caixiashan, Hongyuan, Hongxingshan and Yuxi (Lu et al., 2012; Li et al., 2016). The Aqishan-Yamansu belt is composed of Carboniferous-Permian basalt, andesite, dacite, volcaniclastic rocks and terrigenous clastic rocks with limestone interbeds (Xiao et al., 2004). Several volcanic-hosted Fe deposits were discovered along the belt, including Yamansu, Kumutag, Bailingshan and Hongyuntan (Hou et al., 2014; Zhang et al., 2015). The Kanggur shear zone contains mainly Carboniferous volcano-sedimentary rocks. Most rocks of the Kanggur shear zone were greenschist-facies metamorphosed and ductile deformed (Xiao et al., 2004). Gold (Chen et al., 2012) and Cu-Ni sulfide deposits (Mao et al., 2008) were discovered in the western and eastern parts

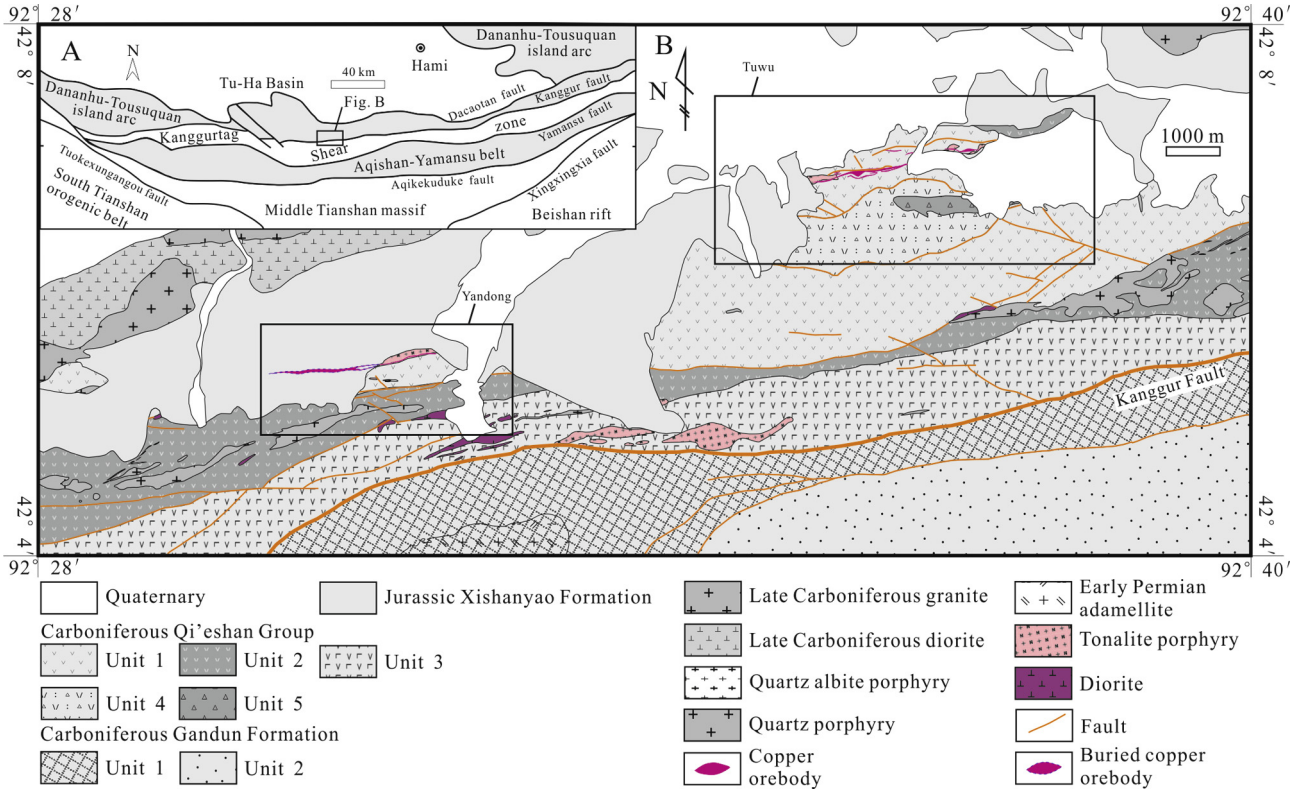

Fig. 1. (A) Tectonic subdivision of Eastern Tianshan (Han et al., 2006); (B) Geologic map of the Tuwu-Yandong Porphyry Cu belt (Shen et al., 2014a).

of the belt, respectively. The Dananhu-Tousuquan arc comprises Devonian to Carboniferous volcanic and intrusive rocks, and hosts important porphyry copper deposits, such as Yandong, Tuwu, Linglong, Chihu and Fuxing (Wu et al., 2006; Shen et al., 2014b). The Harlik arc contains Devonian-Carboniferous calc-alkaline mafic to felsic lavas, volcaniclastics, tuffs, flysch and Ordovician to Permian granitic intrusions (Mao et al., 2014).

3. Ore deposit geology

3.1. Tuwu-Yandong Cu belt

The Tuwu-Yandong Cu belt is located at about 1–4 km north of the Kanggur Fault (Fig. 1B). Major lithostratigraphic units are the Devonian to Carboniferous Qi'eshan Group and the Jurassic Xishanyao Formation (Fig. 1B). The Qi'eshan Group is S-dipping at 43–63°, generally with well-developed schistosity (#1 XJBGMR, 2012). The group (ca. 600–2000 m thick) comprises five units. The lowermost unit is composed of basalt intercalated with andesite, dacite and tuff, which are overlain by pebbly sandstone intercalated with basalt and andesite (the fourth unit). The third unit is composed of pebbly sandstone – volcaniclastic breccia interbeds overlain by lava breccias and conglomerate (the second unit) and the uppermost polymict conglomerate. The basalt flows are generally porphyritic with phenocrysts of plagioclase with minor augite, biotite and amphibole, and a groundmass of plagioclase with minor magnetite. The andesite is also porphyritic but the phenocrysts and groundmass are typically plagioclase with minor amphibole and quartz. Previous studies indicated that the Qi'eshan Group basalt and andesite were formed during ca. 390–360 Ma (Rui et al., 2002) and may have been subduction-related (Zhang et al., 2006; Shen et al., 2014b). The basalt and andesite are generally altered by chlorite, epidote, carbonate, and sulfide alterations. The Jurassic Xishanyao Formation is composed of sandstone, siltstone, mudstone, and conglomerate, and overlie the Qi'eshan Group along an angular unconformity (Wang et al., 2015).

3.2. Yandong Cu deposit

In the vicinity of Yandong, the Qi'eshan Group is intruded by the diorite, tonalite porphyry, quartz albite porphyry (granitic) and quartz porphyry. The diorite is composed of plagioclase (>90 vol. %) and amphibole (5–10 vol.%) with accessory zircon. The widely-distributed and ore-bearing tonalite porphyry contains 35–45 vol.% plagioclase, 25–35 vol.% quartz and about 5 vol.% biotite with accessory zircon and apatite. The less-common quartz albite porphyry (granitic) contains 30–40 vol.% albite and 30–45 vol.% quartz with accessory zircon and apatite. The quartz porphyry mainly occurs south of Yandong (Fig. 2).

The Yandong Cu deposit is mainly controlled by E-, NW- and NE-trending faults (Fig. 2) and contains mainly disseminated and veinlet ores. No distinct boundary exists between the orebodies and the wall rock, and orebodies are delineated with a nominal cut-off grade of 0.50% Cu. The main orebody at Yandong extends for over 3000 m

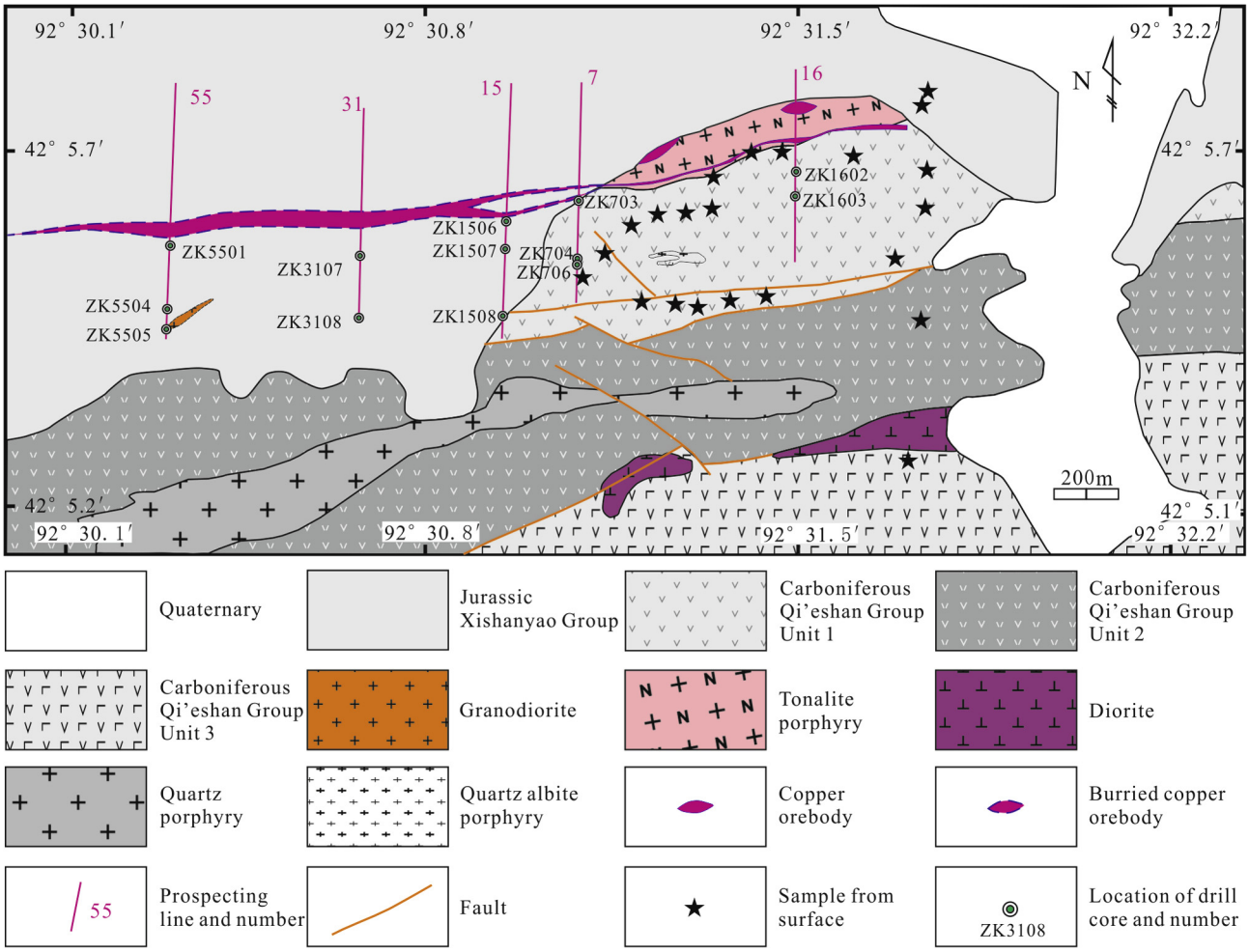

Fig. 2. Geologic map of the Yandong deposit (#1XJBGMR, 2012).

long and ca. 10–50 m wide (Fig. 2). It dips steeply to the south at 68–88°. At Yandong, about 80% and 20% of the Cu ore is hosted in the tonalite porphyry and the Qi'eshan Group (Unit 1), respectively (Fig. 3). Ore minerals include mainly pyrite, chalcopyrite and molybdenite, with minor bornite, chalcocite, magnetite, sphalerite and galena. Non-metallic minerals are mainly composed of quartz, sericite, chlorite, epidote, anhydrite, gypsum, and calcite.

3.3. Paragenetic relationships

Alteration types and zonation at the Yandong Cu deposit have been interpreted differently by previous researchers (Rui et al., 2002; Li et al., 2006; Shen et al., 2014a; Zhang et al., 2010). Rui et al. (2002) divided the alteration zonation of the Yandong Cu deposit into propylitic, biotite and quartz-sericite zones from wall rock to the tonalite porphyry, with carbonate and anhydrite alterations locally developed, and the Cu orebody is mainly located in the biotite and quartz-sericite zones. Li et al. (2006) suggested that the alteration outwards from the Center of the deposit could been divided into strong silication, biotitization, quartz-sericite, argillization and propylitic zones, and silication, biotitization, quartz-sericite alterations closely related to Cu mineralization. Zhang et al. (2010) described the alteration outwards from the Center of the deposit as four zones, i.e., potassic, phyllic, chlorite-

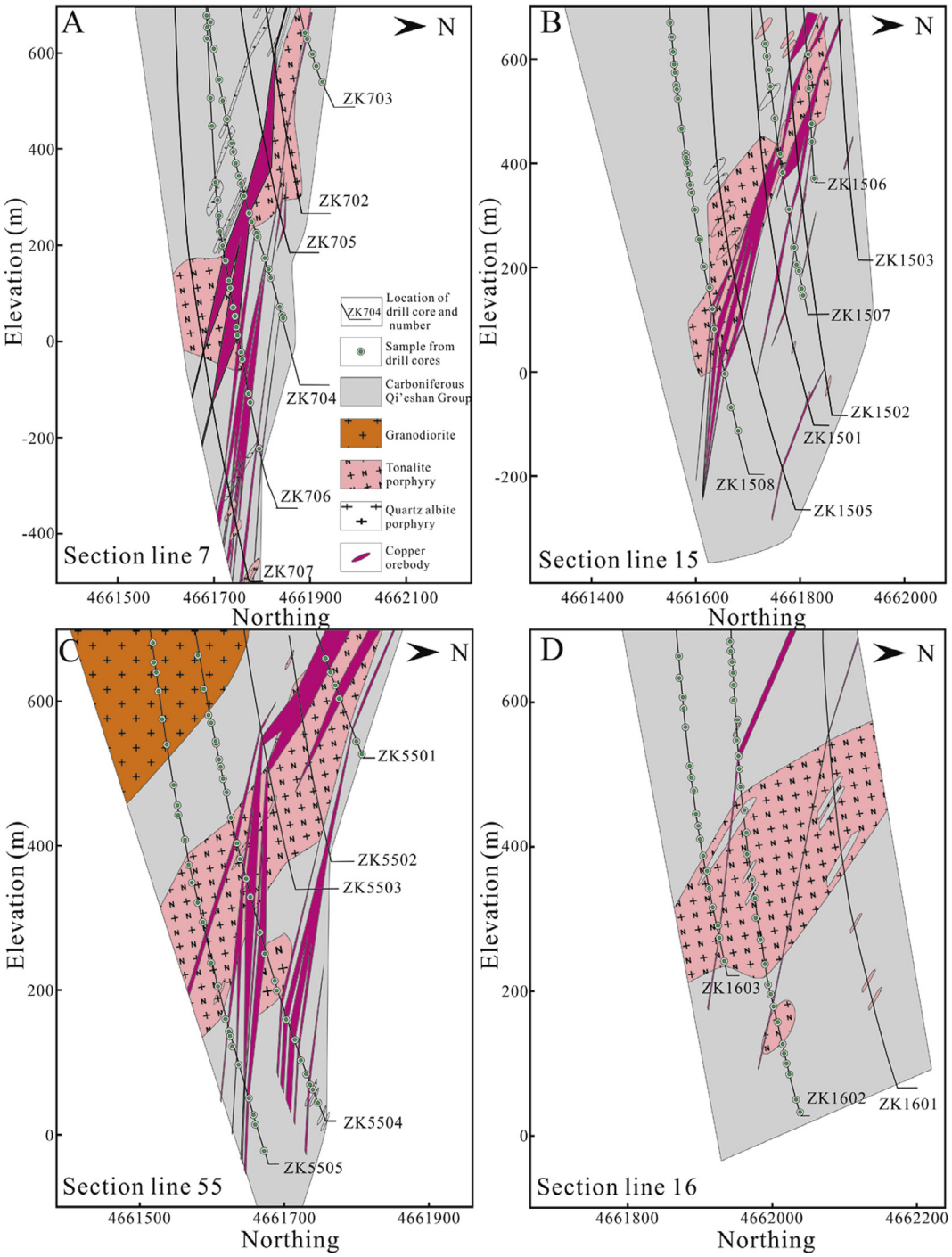

Fig. 3. Cross sections along Exploration Lines 7, 15, 55 and 16 of the Yandong Cu deposit, showing the sampling locations (#1XJBGMR, 2012).

biotite and propylitic zone, and the Cu orebody is mainly located in the phyllic zone. Different from the previous studies, Shen et al. (2014a) reported that two independent alteration and mineralization porphyry systems developed at the Yandong Cu deposit: early-stage andesite porphyry system and late-stage tonalite porphyry system, and the tonalite porphyry system produced approximately 70% Cu. On the basis of megascopic and microscopic textural relationships and mineral assemblages, we have divided the hydrothermal alteration and mineralization of the Yandong Cu deposit into porphyry mineralization (including propylitic alteration, quartz-magnetite alteration and phyllic alteration stages), overprinting (including overprinting mineralization and late vein stages) and supergene periods (Fig. 4, Xiao et al., 2016; Wang et al., 2016). Unlike typical porphyry Cu deposits, potassic alteration is not well developed at Yandong. Hypogene Cu mineralization occurred mainly in the overprinting period and minor in the porphyry mineralization period (Wang et al., 2016; Xiao et al., 2016), during which Cu was deposited mainly as chalcopyrite with minor bornite.

Stage I: Propylitic alteration is most widely present in the Qi'eshan Group (Fig. 5A), and contains mainly chlorite, epidote, calcite and quartz with minor sphene and apatite (Fig. 5B). Propylitically altered rocks generally appear light green in hand specimens. Epidote and chlorite extensively replaced mafic minerals (e.g., amphibole, pyroxene and biotite), and sulfides were rarely found. Multiple vein types exist at this stage, such as chlorite, calcite, epidote ± quartz and quartz ± chlorite veins. Based on crosscutting relationships (Fig. 5C), at least part of propylitic alteration at Yandong occurred before Stage II quartz-magnetite veins.

Stage II: Major quartz-magnetite alteration minerals are magnetite and quartz and minor biotite and pyrite. Magnetite commonly occurs in the magnetite + quartz veins (Fig. 5C), which crosscut the propylitic-altered Qi'eshan Group volcanic rocks and the tonalite porphyry. The magnetite-quartz veins were extensively overprinted by later veins and alteration events (Fig. 5D), and are mainly preserved at deep parts of the mine (often 500 m below the ground).

Stage III: Phyllic alteration affected in the tonalite porphyry and its surrounding Qi'eshan Group volcanic wall rocks, with the feldspars being partly to completely sericitized. Major alteration/mineralization minerals include sericite + quartz + pyrite ± chalcopyrite ± molybdenite. Sulfide + quartz + sericite veins are common (Fig. 5E and F). Qin et al. (2002) reported a sericite K-Ar age of 341.0 ± 4.9 Ma for the phyllic altered rocks, which is coeval with the tonalite porphyry (ca. 339 Ma; Xiao et al., 2016), indicating that the phyllic alteration, early Cu mineralization and tonalite porphyry may have been related.

Stage IV: The overprinting mineralization is featured by chalcopyrite + chlorite + anhydrite + calcite, and intersect the phyllic alteration in the early porphyry mineralization (Fig. 5G). In the quartz + pyrite + chalcopyrite veins of the tonalite porphyry (Fig. 5E), pyrite and sericite were replaced by chalcopyrite + chlorite + anhydrite + calcite (Fig. 5H). The mineral assemblage of chalcopyrite + chlorite + anhydrite + calcite was also found in the quartz albite porphyry (granitic) (Fig. 5I). Chalcopyrite-molybdenite intergrowth was identified at this stage (Fig. 5J), suggesting that molybdenite occurs at both Stages III and IV, which is consistent with the two molybdenite re-Os age clusters of ca. 341–

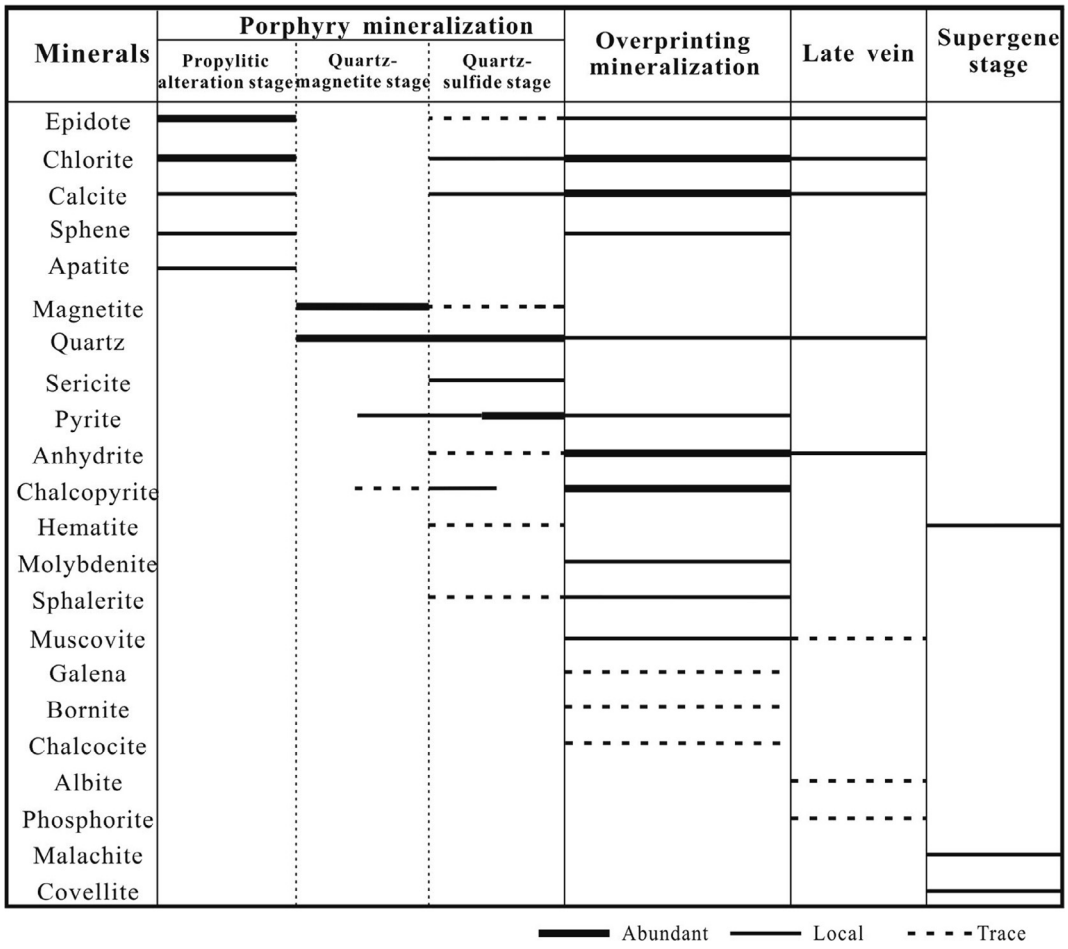

Fig. 4. Alteration and mineralization paragenesis of the Yandong Cu deposit.

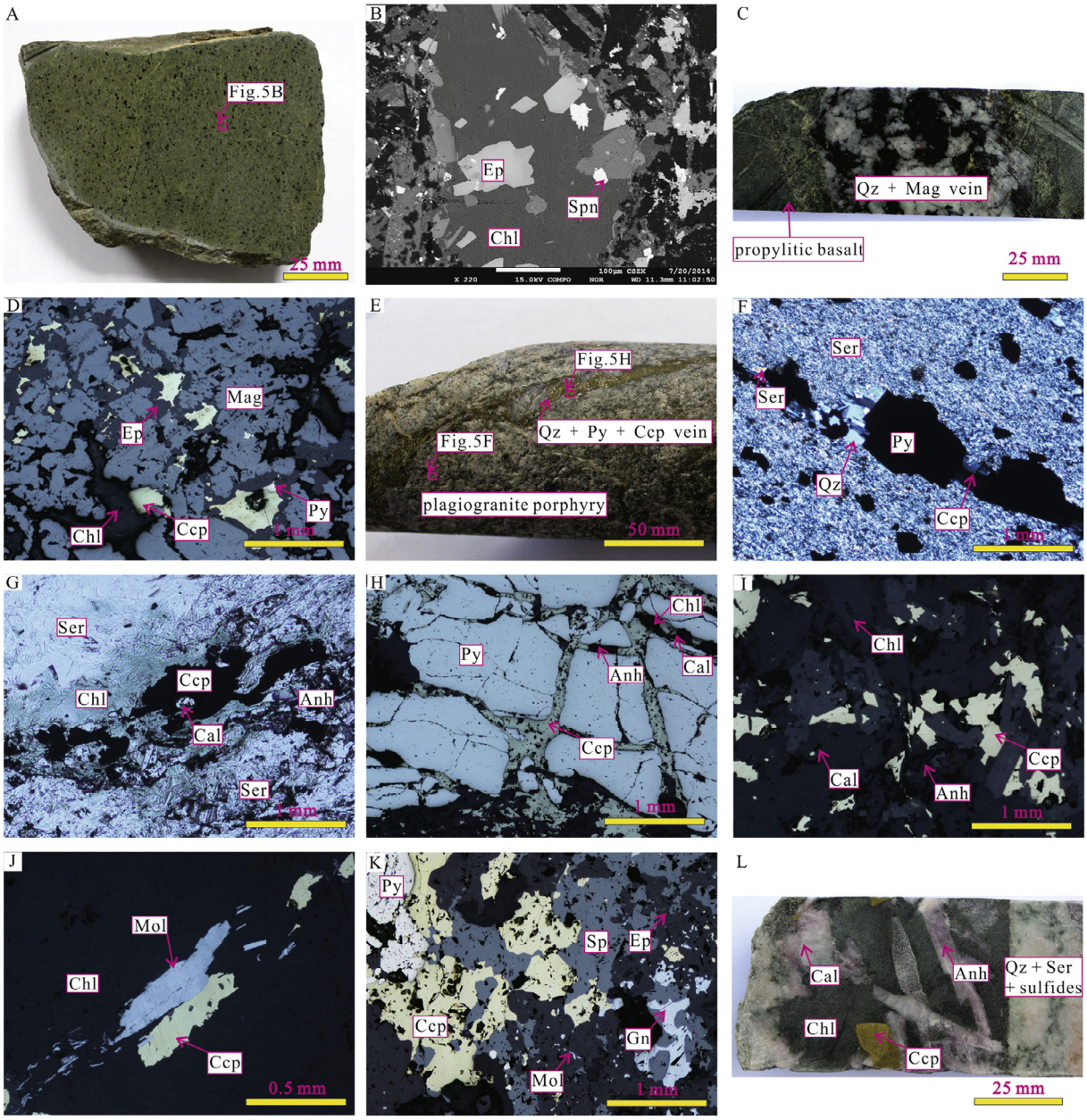

Fig. 5. Representative hand specimen photographs and microphotographs of the Yandong Cu deposit. (A) Propylitic-altered Qi'eshan Group basalt; (B) BSE image illustrating the replacement of mafic minerals in basalt by chlorite + epidote + sphene; (C) Quartz + magnetite vein cut propylitic-altered basalt; (D) Quartz + magnetite vein replaced by epidote + chalcopyrite + chlorite + pyrite; (E and F) Phyllic-altered tonalite porphyry; (G) Chalcopyrite + chlorite + anhydrite + calcite intersect phyllic alteration; (H) Quartz + sulfide vein in phyllic-altered tonalite porphyry replaced by chalcopyrite + chlorite + anhydrite + calcite; (I) Chalcopyrite + chlorite + anhydrite + calcite in quartz albite porphyry (granitic); (J) Chalcopyrite intergrown with molybdenite at Stage IV; (K) Chalcopyrite + pyrite + epidote + sphalerite + galena + molybdenite at Stage IV; (L) Stage IV coarse chalcopyrite + chlorite + anhydrite + calcite intersect quartz + sericite + sulfides. Abbreviations: Anh, anhydrite; Cal, calcite; Ccp, chalcopyrite; Chl, chlorite; Ep, epidote; Mag, magnetite; Mol, molybdenite; Py, pyrite; Qz, quartz; Ser, sercite; Sp, sphalerite; Spn, sphene; Gn, galena.

334 Ma (Zhang et al., 2008) and ca. 323 Ma (Rui et al., 2002). The chalcopyrite + pyrite + epidote + sphalerite + galena + molybdenite assemblage is also rarely found at Stage IV (Fig. 5K). In this study, we also newly identify a coarse chalcopyrite + chlorite + anhydrite + calcite assemblage (that crosscut quartz + sericite + sulfides) (Fig. 5L), which is markedly different from typical porphyry Cu mineralization (dominated by quartz + sulfides stockwork; Sillitoe, 2010).

Stage V: Late veins include ore-barren quartz + calcite + anhydrite, quartz + calcite + epidote, calcite, anhydrite ± calcite and quartz + albite veins with ambiguous relative age relationships.

Stage VI: Supergene mineralization is represented by oxidized minerals, including malachite, hematite and covellite.

4. Samples and analytical methods

In this study, 22 outcrop samples and 267 drill core samples (from 13 holes) were collected. Stage I chlorite samples were mostly from outcrops (a few from drill cores) in the Exploration Line 16 (Figs. 2 and 3) and Stage IV chlorite samples were all from drill cores. Over 300 polished thin sections were prepared and studied using transmitted and reflected light microscopy, and representative samples were then examined with EMPA and LA-ICP-MS to aid mineral identification and mineralogical studies.

Chlorite and epidote major element analyses were conducted using a Cameca SX100 electron microprobe at the Testing Center of Shangdong Bureau of China Metallurgical Geology Bureau and

the Guangzhou Institute of Geochemistry (GIG), Chinese Academy of Sciences (CAS) with a JEOL JXA-8230 Superprobe and a JEOL JXA-8100 Superprobe, respectively. Major and trace elements of chlorite and epidote were determined by a pulsed Resonetic 193 nm Laser Ablation system coupled with an Agilent 7500a ICP-MS at the GIGCAS. Detailed operating conditions for the laser ablation system and the ICP–MS instrument and data reduction were described in Liu et al., (2008). The operating conditions are as follows: 15 kV accelerating voltage, 20 nA beam current, 1 μm beam diameter, 10 s counting time and ZAF correction procedure for data reduction. For the same mineral, the analytical results from two laboratories were compatible. Back-scattered electron (BSE), energy dispersive spectrometer (EDS) and multi-element imaging with a field emission gun scanning electron microscope (FEG-SEM) were undertaken with an acceleration voltage of 20 keV and a beam current of 2.9 nA.

Concentrations of 53 elements (Li, B, Na, Mg, Al, Si, Fe, K, Ca, Sc, Ti, V, Cr, Mn, Co, Ni, Cu, Zn, Ga, As, Rb, Sr, Y, Zr, Nb, Mo, Ag, Sn, Sb, Cs, Ba, La, Ce, Pr, Nd, Sm, Eu, Gd, Tb, Dy, Ho, Er, Tm, Yb, Lu, Hf, Ta, Au, Tl, Bi, Pb, Th, and U) were determined in chlorite and epidote by LA-ICP-MS at the GIGCAS, following the analytical protocol of Wilkinson et al. (2015). Chlorite was ablated using spot sizes ranging from 40 to 60 μm (depending on grain size and presence of inclusions) using a pulse energy density of ca. 8.0 J/cm^2 and pulse repetition rate of 10 Hz. The concentrations of 53 elements were determined during each analysis, which consisted of an initial 30 s to measure the gas blank followed by up to 60 s of sample ablation, for a total analysis time of 90 s. Analyses were calibrated using two external standards (NIST 612 and BHVO), and the FeO and CaO contents determined by EMPA were used as internal standardization for chlorite and epidote, respectively.

5. Results

5.1. Data filtering

Chlorite and epidote could have complex structures, and commonly contain mineral inclusions and coexist with other minerals. Consequently, it is necessary to evaluate these potential contaminating effects on the EPMA and LA-ICP-MS data obtained. As suggested by Foster (1962) and Inoue et al. (2010), contaminated chlorites typically have elevated ($CaO + Na_2O + K_2O$) > 0.5 wt.%, and therefore only the chlorite data with ($CaO + Na_2O + K_2O$) ≤ 0.5 wt.% were used in this study. Normal chlorite contains Si = 100,000–225,000 ppm, K ≤ 1000 ppm, Ti ≤ 1000 ppm and Zr ≤ 2 ppm, and normal epidote contains Na ≤ 1000 ppm, K ≤ 1000 ppm and Ti ≤ 1000 ppm (P1060 analytical and data reduction protocol, CODES). In this study, we excluded the chlorite and epidote data with compositions outside these composition ranges.

In this study, 3–5 chlorite and 2–3 epidote EPMA, 3–5 chlorite and 3–5 epidote LA-ICP-MS data have been analyzed on every selected samples. Finally, 237 chlorite and 139 epidote EPMA data, and 264 chlorite and 207 epidote LA-ICP-MS data have been obtained with 16 abnormal chlorite EPMA data, and 85 abnormal chlorite and 76 abnormal epidote LA-ICP-MS data excluded. The contents of SiO_2, Al_2O_3, FeO and MgO of chlorite, and the contents of SiO_2, Al_2O_3, FeO and CaO of epidote were from EMPA, and those of other elements were from LA-ICP-MS.

5.2. Major element chemistry

Chlorite EMPA results are listed in Appendix I. Stage I chlorite (Chl-1) contains SiO_2 = 26.75–31.91 wt.%, Al_2O_3 = 16.00–22.30 wt.%, FeO = 9.47–21.01 wt.% and MgO = 19.21–26.83 wt.%, with Fe/(Fe + Mg) = 0.17–0.37 (Appendix I). Comparatively, Stage IV chlorite (Chl-2) contains lower SiO_2 (22.41–29.65 wt.%) and MgO (7.78–20.51 wt.%), but higher FeO (16.71–34.57 wt.%), Al_2O_3 (15.89–24.36 wt.%) and Fe/(Fe + Mg) ratios (0.31–0.71). The contents of Cr_2O_3, TiO_2, CaO, K_2O, P_2O_3 and Na_2O for both the Chl-1 and Chl-2 are uniformly low. Chlorite analyses are recalculated on the basis of 14 oxygen atoms per formula unit (a.p.f.u) and are plotted on the chlorite classification diagram (Fig. 6; Deer et al., 1962). Chl-1 mainly falls in the pycnochlorite field (Si values = 2.74 to 3.17 (a.p.f.u) and total Fe (i.e., Fe^{2+} + Fe^{3+}) values = 0.78 to 1.83 (a.p.f.u). Chl-2 primarily plots in the ripidolite and pycnoclorite fields with Si values = 2.50 to 3.10 (a.p.f.u) and total Fe values = 1.41 to 3.14 (a.p.f.u). $Al^{(IV)}$ contents in the Chl-1 and Chl-2 display strong positive correlation with Fe/(Fe + Mg) ratios, as expressed by the equation: $Al^{(IV)} = 0.79 * Fe/(Fe + Mg) + 0.86$, indicating that replacement of Si by $Al^{(IV)}$ was accompanied by the substitution of Mg by Fe (Monteiro et al., 2008). In the correlation diagram of the main cations in chlorite (Fig. 7), Chl-1 and Chl-2 both exhibit good linear Al vs. Si and Mg vs. Fe relationships.

Epidote EMPA results are listed in Appendix II, which show a wide range of compositions from the epidote end member [$Ca_2Al_3Si_3O_{12}(OH)$] to clinozoisite $Ca_2Al_2Fe^{3+}Si_3O_{12}(OH)$, with X_{Fe} values = 0.14 to 0.40. Stage I epidote (Ep-1) shows significant chemical variation, with SiO_2 = 31.92–41.16 wt.%, Al_2O_3 = 18.43–28.19 wt.%, FeO = 6.36–17.54 wt.% and CaO = 16.75–23.70 wt.%, and Fe/(Fe + Al) = 0.14–0.40. Stage IV epidote (Ep-2) contains similar chemistry with Ep-1 (Fig. 8), with SiO_2 = 28.99–39.84 wt.%, Al_2O_3 = 19.90–29.90 wt.%, FeO = 6.75–15.77 wt.% and CaO = 19.00–23.63 wt.%, and Fe/(Fe + Al) = 0.14–0.36. Contents of Cr_2O_3, MnO, K_2O, TiO_2, P_2O_5 and Na_2O for both Ep-1 and Ep-2 are uniformly low. However, different parts of the same epidote grain shows dramatic compositional variations. In Fig. 9, compared with the dark areas (BSE image), the light areas of epidote have higher FeO and lower Al_2O_3 contents, which may have been related to unstable physicochemical conditions or formation at different stages.

5.3. Trace element chemistry

The mean of trace element concentrations of selected elements for chlorite and epidote were given in Appendix III and IV. In general, the most abundant trace element in Chl-1 and Chl-2 is Mn (1000–10,000 ppm) (Appendix III). Most Chl-1 and Chl-2 have Zn, B, Na, K, Sc, V, Cr,Co, Ni, Cu, Ga, As, Sr, Rb, Ba and Ti contents rang-

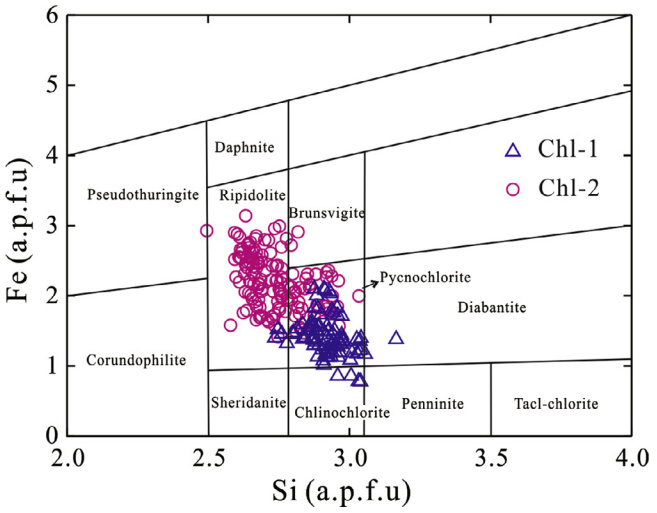

Fig. 6. Chlorite classification diagram (Deer et al., 1962) for the Yandong chlorite.

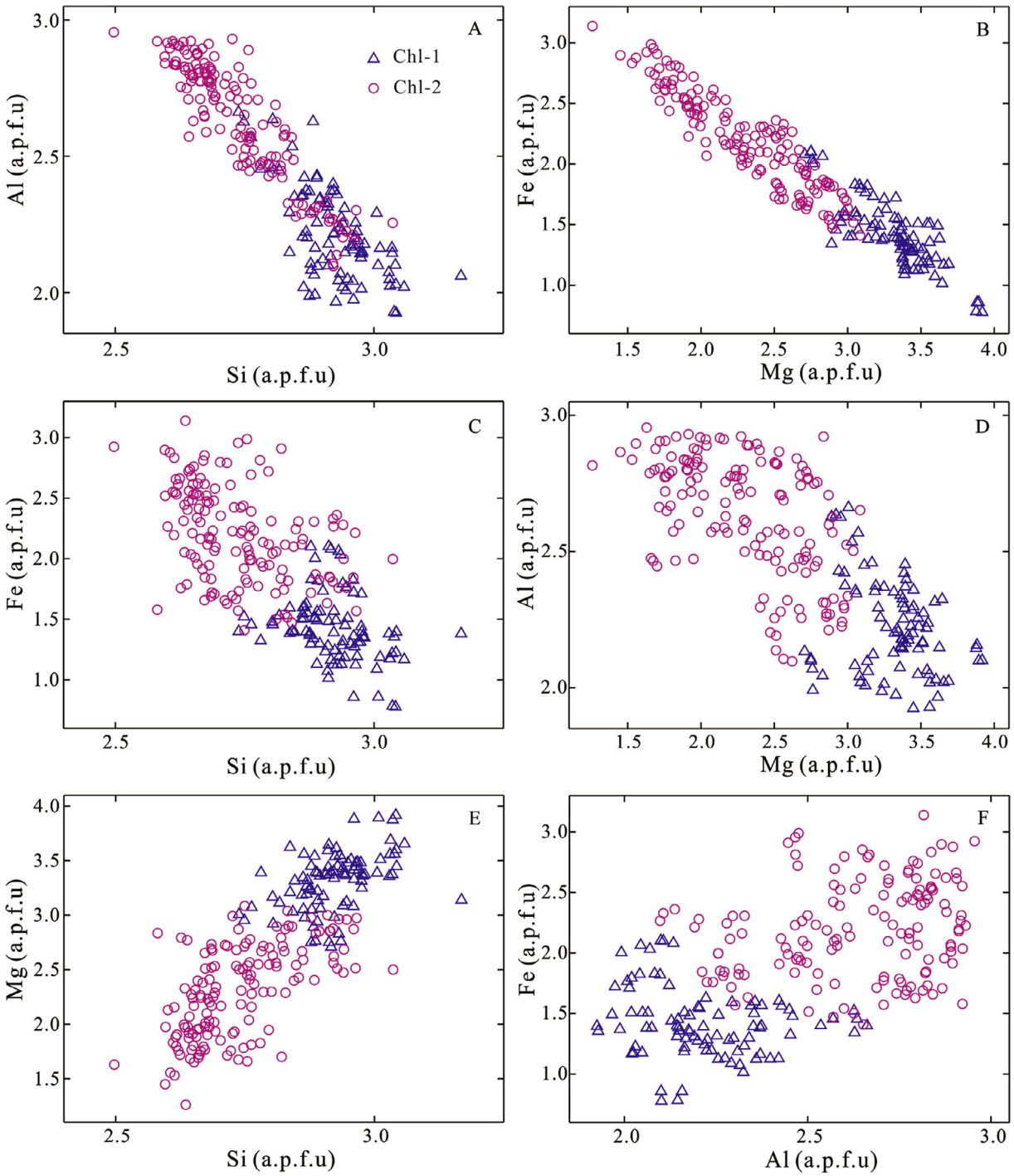

Fig. 7. Binary diagram for the Yandong chlorite. (A) Al (a.p.f.u) vs. Si (a.p.f.u); (B) Fe (a.p.f.u) vs. Mg (a.p.f.u); (C) Fe (a.p.f.u) vs. Si (a.p.f.u); (D) Al (a.p.f.u) vs. Mg (a.p.f.u); (E) Mg (a.p.f.u) vs. Si (a.p.f.u); (F) Fe (a.p.f.u) vs. Al (a.p.f.u).

ing from ~1 to 1500 ppm, or 100 to 1000 times of their respective detection limits, whereas concentrations of other elements, e.g., Y, Zr, Nb, Mo, Ag, Sn, and REEs, are either close to or below the detection limits (Appendix III). Chl-1 contains wide ranges of V (54.6–267 ppm), Cr (23.4–3315 ppm), Mn (1083–4261 ppm), Co (24.9–153 ppm), Ni (206–1175 ppm), Cu (0.47–1671 ppm), Zn (142–949 ppm), Sr (1.87–460 ppm) and Ti (13.1–871 ppm), and Chl-2 also shows large ranges of V (6.91–616 ppm), Cr (1.85–372 ppm), Mn (473–8659 ppm), Co (0.02–159 ppm), Ni (2.27–1662 ppm), Cu (0.24–25,529 ppm), Zn (198–3860 ppm), Sr (0.30–338 ppm) and Ti (23.8–469 ppm). Both Chl-1 and Chl-2 show positive Ga vs. V, Co vs. Ni, and Mn vs. Zn correlations (Fig. 10A, B, C), but negative Sn vs. As correlation (Fig. 10D). Compared with Chl-1, Chl-2 shows higher Sc, Ga, Sn, Ti, Zn and Mn, but lower Cr, Ni, Co, B, Ca and Sr (Fig. 11).

In general, the most abundant trace elements in Ep-1 and Ep-2 are Mn and Sr (>500 ppm). Ep-1 and Ep-2 have B, Na, K, Sc, Ti, V, Cr, Co, Ni, Cu, Zn, Ga, As, Y, Zr, Sn, Sb, Ba, Pb, Hf and REE contents ranging from ~1 to 2000 ppm, or 100 to 1000 times of their respective detection limits (Appendix IV), whereas concentrations of Ag, Mo, Nb, Au, Tl, Bi, Th and U are low (<1 ppm). Ep-1 have large ranges of Sc (1.04–267 ppm), V (118–736 ppm), Cr (3.76–2358 ppm), Cu

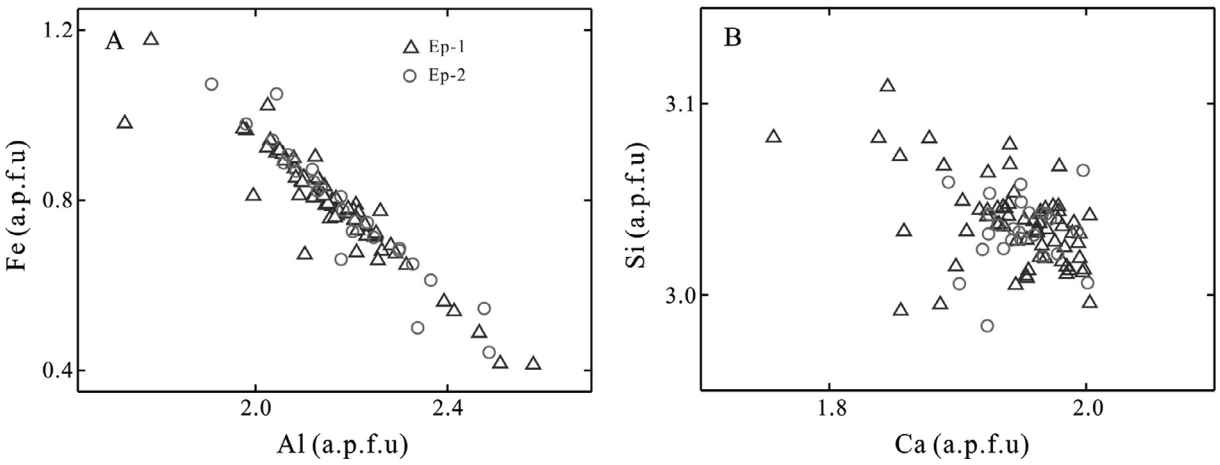

Fig. 8. Binary diagram for the Yandong epidote. (A) Fe (a.p.f.u) vs. Al (a.p.f.u); (B) Si (a.p.f.u) vs. Ca (a.p.f.u).

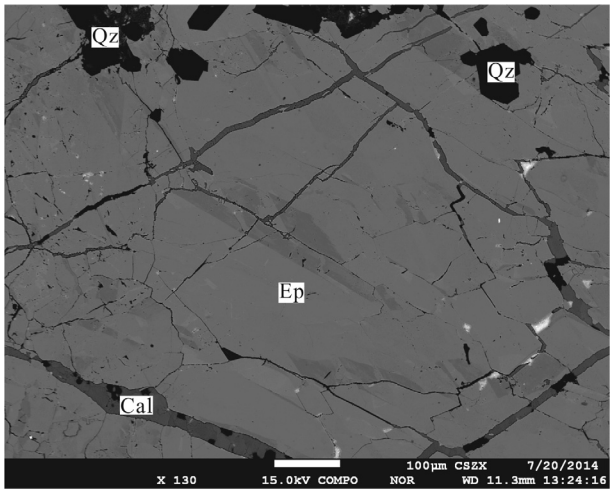

Fig. 9. BSE image showing complex growth zonation in the Yandong epidote.

(0.04–654 ppm), Zn (0.91–204 ppm), As (1.67–656 ppm), Y (1.09–276 ppm), Zr (1.03–244 ppm), Sb (0.33–391 ppm), Ba (0.95–342 ppm) and REE (1–2000 ppm), and Ep-2 also show large ranges of Sc (2.75–138 ppm), V (127–841 ppm), Cr (0.55–1407 ppm), Cu (0.00–12,350 ppm), Zn (1.49–131 ppm), As (5.34–711 ppm), Y (19.1–788 ppm), Zr (0.05–119 ppm), Sb (0.54–1180 ppm) and REE (20–2000 ppm). Compared with Ep-1, Ep-2 contains higher Sn, Y, Ga, Ag, U, Y, Cu and Sr, but lower B, Zr, Ba and Ti (Fig. 12).

6. Discussion

6.1. Chlorite and epidote chemistry of the Yandong Cu deposit

6.1.1. Comparison between Yandong and other deposits

Many Paleozoic porphyry Cu deposits are hosted in metamorphic terranes, which have undergone low temperature, mineralization-unrelated alteration. Therefore, differentiating porphyry Cu mineralization-related propylitic chlorite from unrelated systems is of great exploration significance. Comparing with metamorphic chlorite from Proterozoic metamorphic terranes in Australia, Wilkinson et al. (2015) found that the Batu Hijau (Indonesia) propylitic chlorite contains lower Fe and Li, but higher Mg, Zn, Sb, As, Ag and U. Distal propylitic chlorite is typically depleted in Al, Fe and Li and enriched in Ca, Sr and Si relative to metamorphic chlorite (Wilkinson et al., 2015).

In this study, the Yandong Chl-1 geochemically resembles the Batu Hijau propylitic chlorite. However, the Yandong Chl-2 contains higher Fe, Al and As, but lower Mg and Sn than the Proterozoic metamorphic chlorite in Australia (Fig. 13). We found that Chl-2 coexists with chalcopyrite, anhydrite and calcite in veins, which is clearly different from metamorphic chlorite, indicating another type of hydrothermal chlorite. Hence, chlorite chemistry can not only be used to distinguish porphyry mineralization-related propylitic chlorite from metamorphic chlorite, but also variable types of hydrothermal-related chlorite.

Ep-1 is geochemically similar with the epidote from the porphyry and skarn deposits in the central Baguio district (Philippines) (Cooke et al., 2014). However, the Yandong Ep-2 contains higher Sn, Ga and U, but lower Zr, Ti and Ba than the Baguio epidote (Fig. 14), which also suggests hydrothermal system different from porphyry systems.

6.1.2. Spatial variations of chlorite and epidote compositions

Previous epidote and chlorite geochemical research revealed trace element composition changes at different distances (lateral and vertical) from young porphyry orebodies, e.g., Batu Hijau (ca. 3.7 Ma) (Cooke et al., 2014; Wilkinson et al., 2015). At Batu Hijau, Wilkinson et al. (2015) found that K, Li, Mg, Ca, Sr, Ba, Ti, V, Mn, Co, Ni, Zn and Pb, are probably incorporated into the propylitic chlorite lattice and display systematic spatial variations from the porphyry hydrothermal center: Ti, V and Mg concentrations decrease exponentially with increasing distance, whereas K, Li, Ca, Sr, Ba, Mn, Co, Ni, Zn and Pb concentrations increase. Such chlorite spatial variations extend to at least 4.5 km from the porphyry orebody, giving a much larger footprint than whole rock geochemical anomalies (≤1.5 km). Wilkinson et al. (2015) proposed that the spatial variations in chlorite trace element ratios (e.g., Ti/Sr) can be expressed by the formulae: $x = \ln(R/a)/b$, where x is the distance (m), R is the element ratio, and a and b are exponential fit parameters. LA-ICP-MS analyses on propylitic epidote from the Baguio porphyry and skarn deposits shows highest Cu, Mo, Au and Sn concentrations close to the potassic alteration zone, enrichments in As, Sb, Pb, Zn and Mn at >1.5 km from the deposit center, and enrichments in REEs and Zr along the edge of the pyrite halo (Cooke et al., 2014). Although the Yandong Cu deposit is not a typical porphyry system, its chlorite and epidote chemical spatial variation patterns are similar with those of the world-class porphyry systems abovementioned.

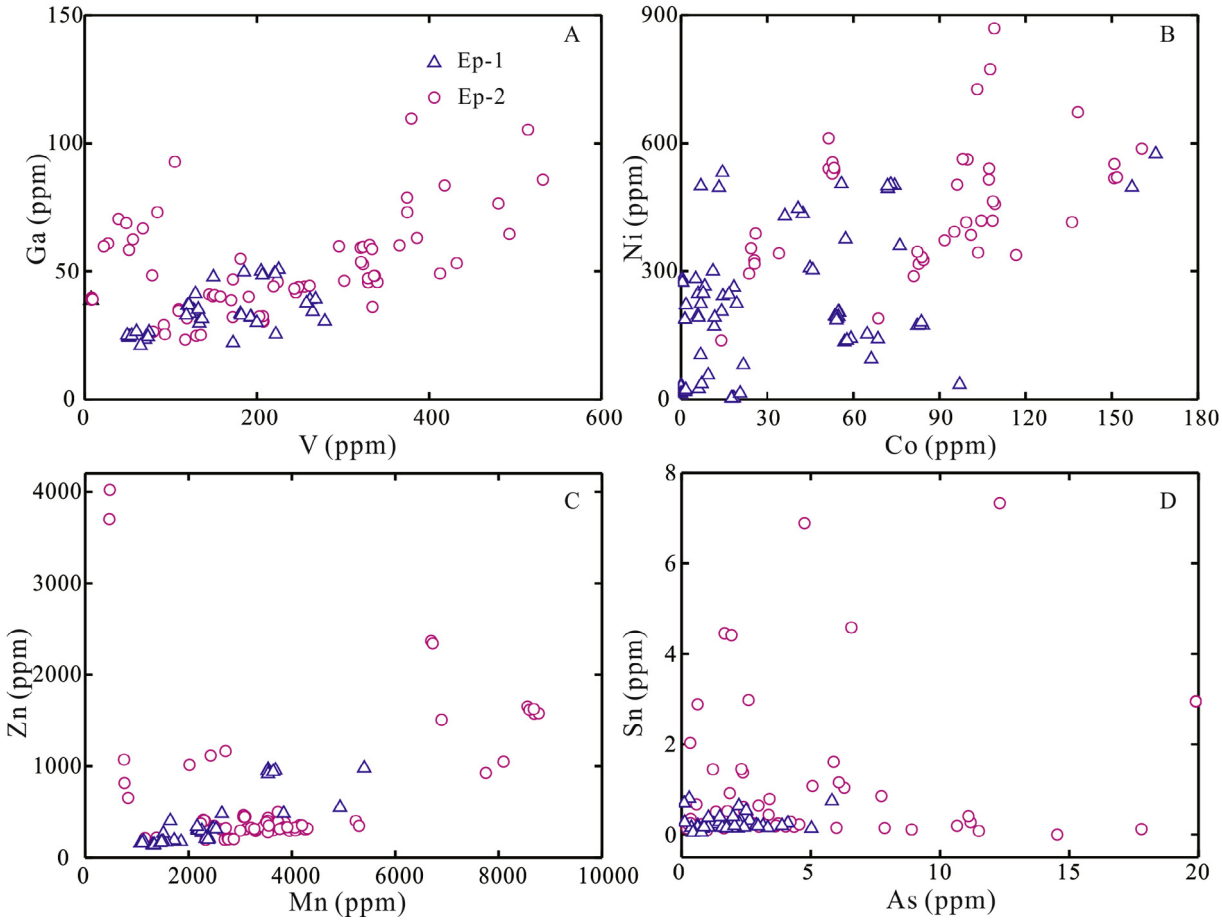

Fig. 10. Binary diagram for the Yandong chlorite. (A) Ga vs. V; (B) Ni vs. Co; (C) Zn vs. Mn; (D) Sn vs. As.

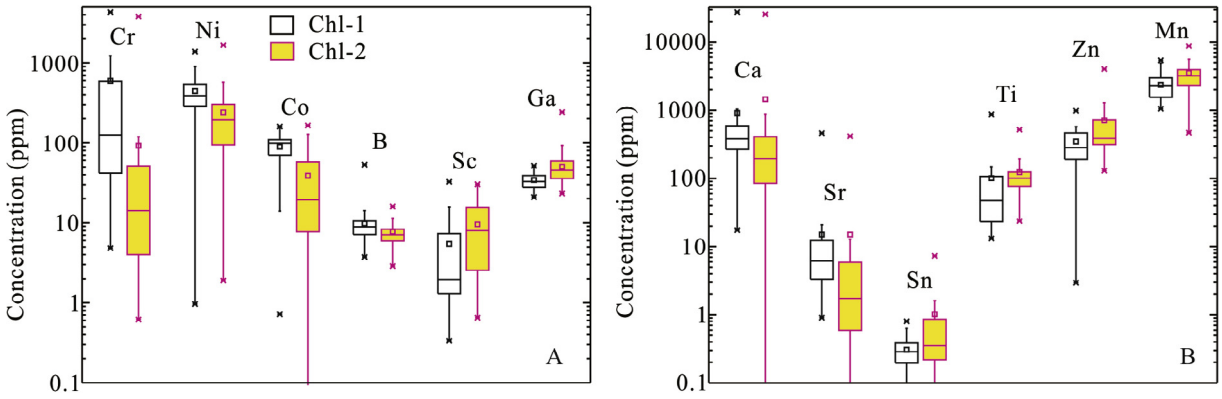

Fig. 11. Geochemical comparison between the Yandong chlorite Chl-1 and Chl-2.

Our new Yandong chlorite data show that most elements have similar spatial variation patterns, despite that Chl-1 and Chl-2 were formed at different stages, e.g., titanium contents are most elevated in both Chl-1 and Chl-2 near the orebody (Appendix V). Wilkinson et al. (2015) argued that temperature is the principal control of Ti concentration in chlorite, which increases with increasing temperature, indicating that the hydrothermal centers of both Stages I and IV are all close to the orebody, which is consistent with the presence of the ore-forming quartz albite porphyry (granitic) and tonalite porphyry there. Although the granodiorite samples were collected far away from the orebody, the anomalous chlorite in granodiorite with high Ti contents may have been generated by the heat sourced from the granodiorite (Fig. 15). Chlorite samples from the bottom of the drill hole ZK1602 (Exploration Line 16) contain high Ti content, which may reveal another hydrothermal center or orebody at depth (Fig. 15). Similar to the case of Batu Hijau (Wilkinson et al., 2015), vanadium concentrations in both Chl-1 and Chl-2 are most elevated near the orebody (Appendix V). Zinc content of chlorite increases exponentially with increasing distance from the Batu Hijau orebody, while Zn in the Yandong Chl-1 and Chl-2 are the highest near the orebody (Appendix VI). Besides, As, Sc and Cu in both Chl-1 and Chl-2 are most elevated near the orebody as well (Appendix VII, VIII and IX); Au and Sn in Chl-2 are most elevated near the orebody and very low or below

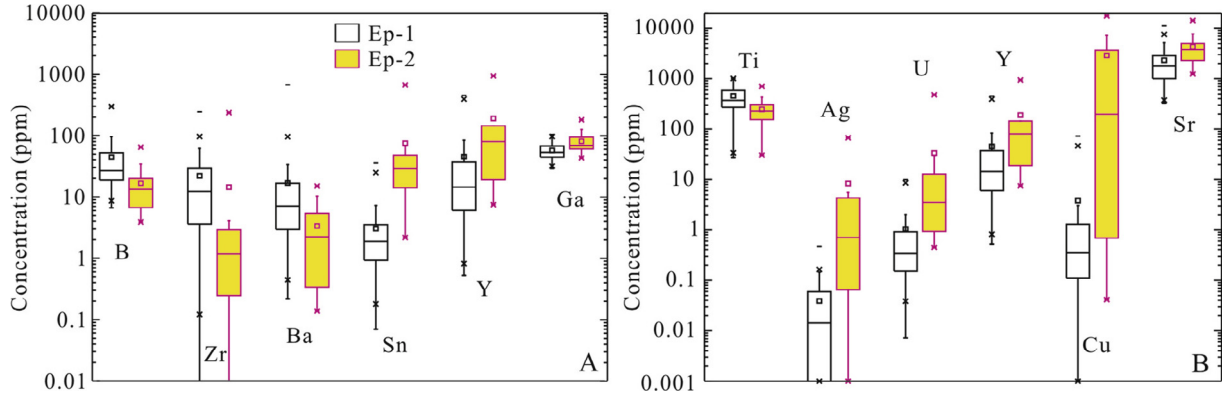

Fig. 12. Geochemical comparison between the Yandong epidote Ep-1 and Ep-2.

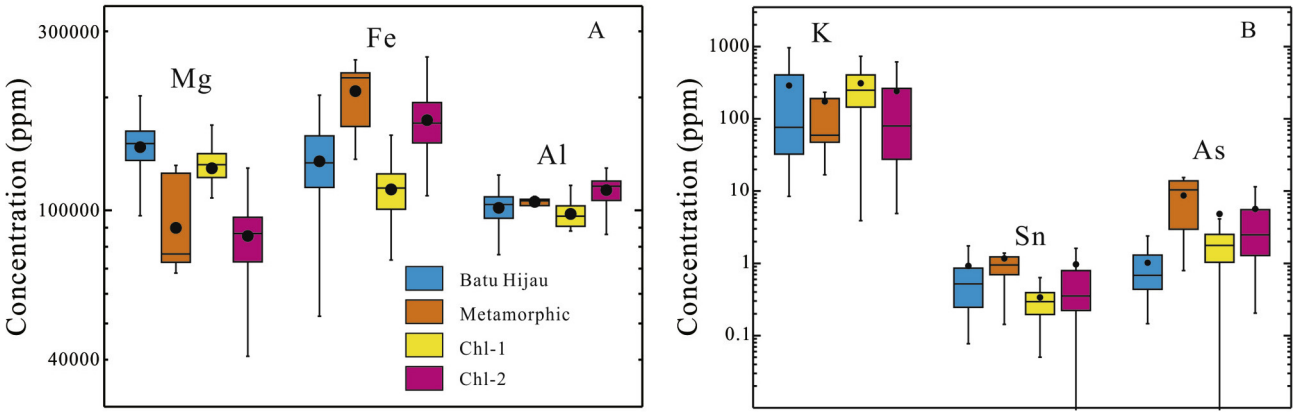

Fig. 13. Geochemical comparison among the Yandong chlorite (Chl-1 and Chl-2) and the Batu Hijau chlorite and metamorphic chlorite from two Proterozoic metamorphic terranes in Australia (Wilkinson et al., 2015).

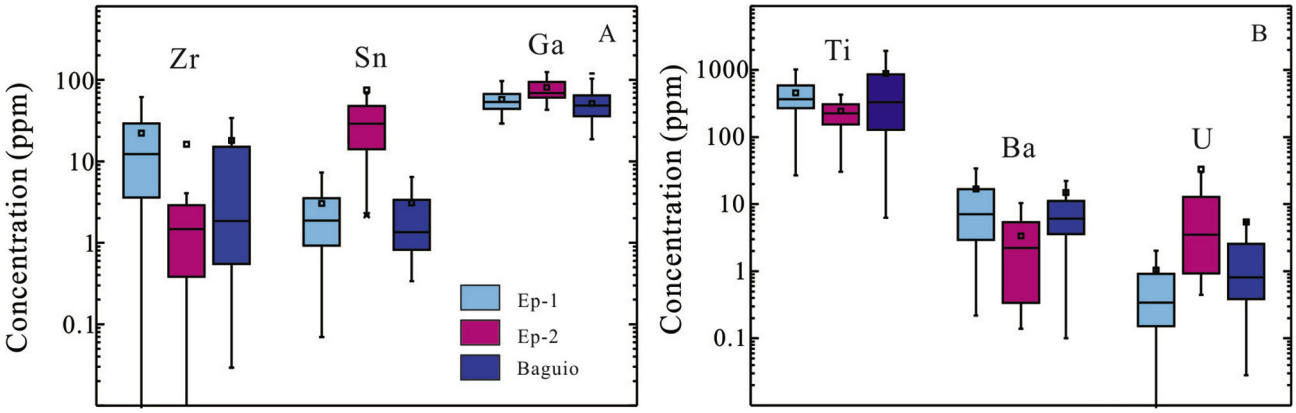

Fig. 14. Geochemical comparison between the Yandong epidote (Ep-1 and Ep-2) and the Baguio epidote.

detection limits away from orebody, but these trends are not obvious in Chl-1 (Appendix X and XI); while Au, Sn, As, Sc and Cu contents of chlorite do not show obvious change patterns in Batu Hijau. Propylitic chlorite from Batu Hijau show that large ion lithophile element (LILE, such as K, Ca, Sr and Ba) concentrations increase with increasing distance from the orebody (Wilkinson et al., 2015), a trend not observed in the Yandong chlorite, which may have been related to LILEs remobilization, due to the late tectonic activities at Yandong Cu deposit. Therefore, LILEs should be used with caution for Paleozoic porphyry Cu exploration.

Ep-2 is not well-developed and is mainly confined near or inside the orebody, and thus chemical spatial variation trend of Ep-2 is not obvious. Therefore, in this study we have focused on the element spatial variation pattern of Ep-1. The Yandong Ep-1 shows the highest Ti and the lowest Sc and Zr contents near the orebody, which is different from the Baguio epidote (Fig. 16A–C). Antimony in Ep 1 is mostly low near the orebody, similar to the Baguio epidote (Fig. 16D). However, these chemical variation patterns are not obvious in the Yandong Exploration Lines 7, 15, 16 and 55, which may have been related to the overprinting alter-

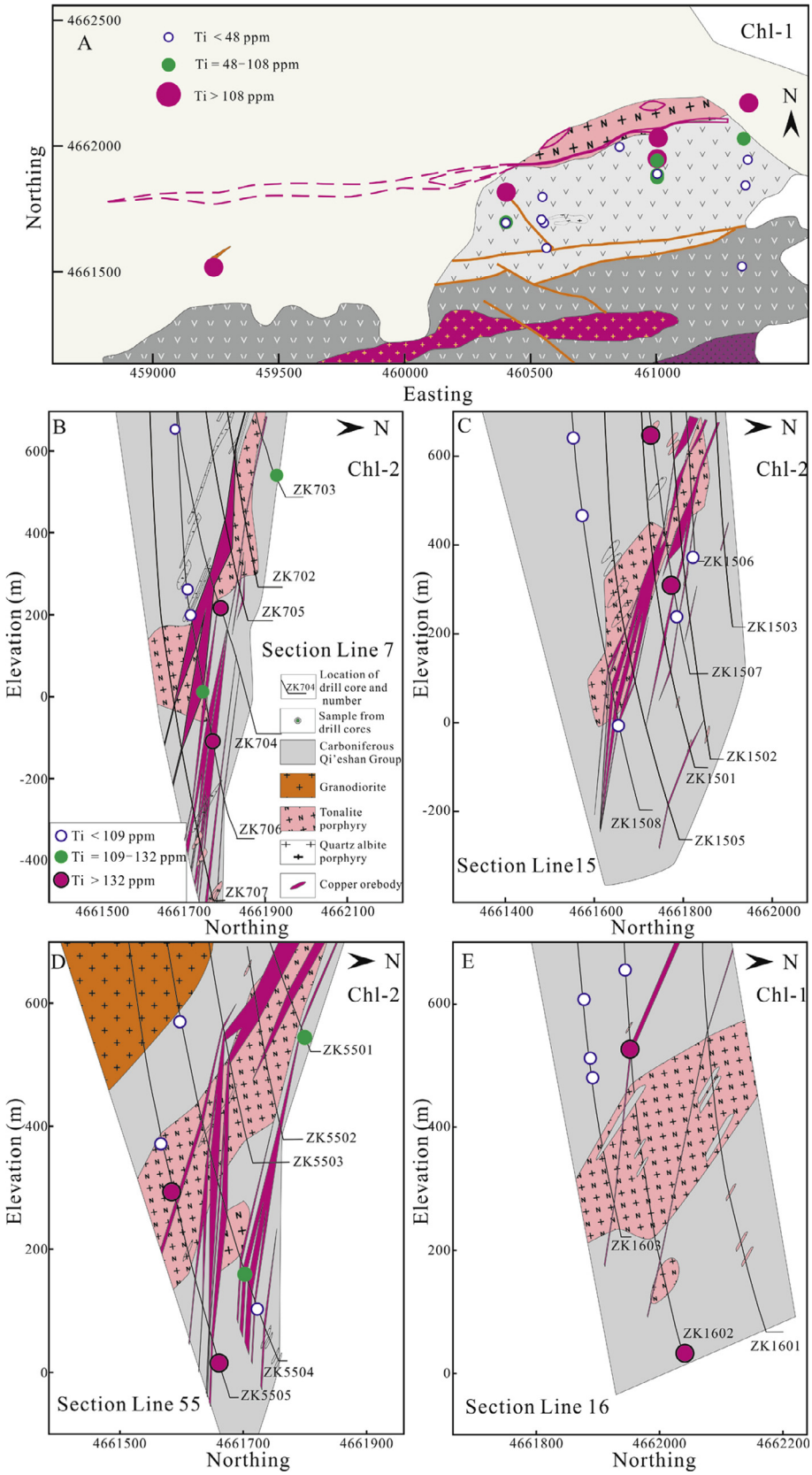

Fig. 15. Spatial distribution of Ti for the Yandong chlorite.

ation. The spatial variation patterns of Cu, Mo, Au, Sn, As, Pb, Zn, Mn and REE in Baguio (Cooke et al., 2014) are not present at Yandong.

LA-ICP-MS analyses of epidote and chlorite reveal that trace elements of chlorite (Ti, Zn, As, V, Sc, Cu, Au and Sn) and epidote (Ti, V, Sc and Zr) varies with lateral distance from the center of orebody in

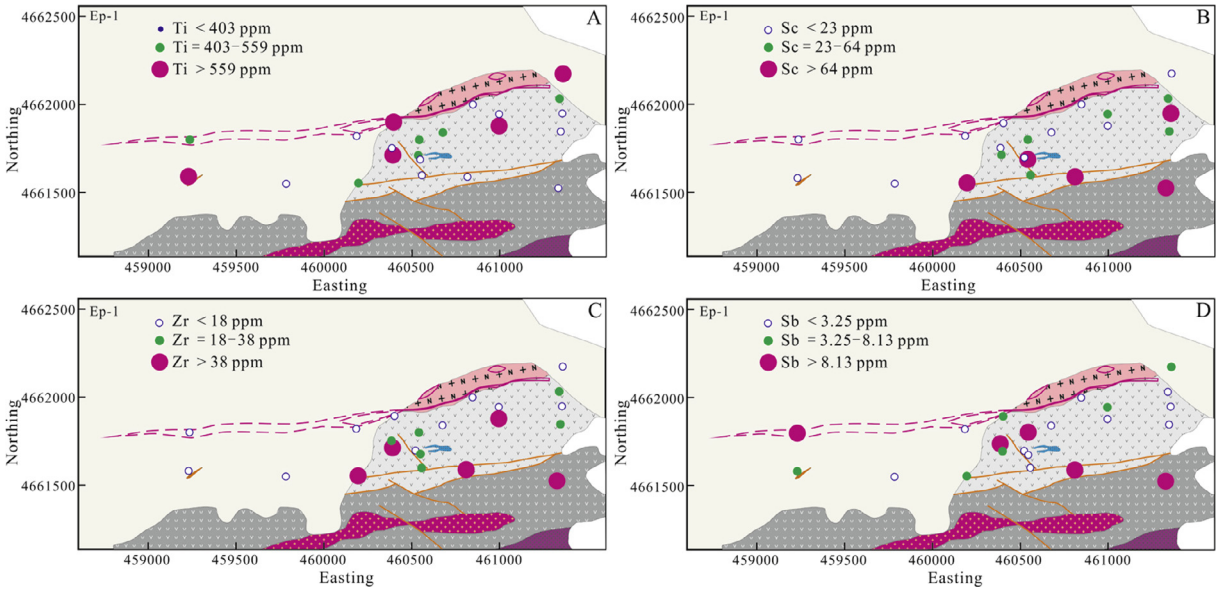

Fig. 16. Spatial distribution of element concentrations for the Yandong Stage IV epidote. (A) Ti; (B) Sc; (C) Zr and (D) Sb contents.

the Yandong Cu deposit. Hence, if multiple samples are available, these patterns can be used to provide a sensitive indicator of direction towards a heat source or orebody. Cooke et al. (2014) found that epidote and pyrite coexist within the pyrite halo where H_2S was abundant, and As, Sb, Pb were preferentially scavenged by pyrite so that their concentrations are low in epidote and suggested that chemical spatial variation trends of epidote are controlled by advective outflow of ascending fluids from the porphyry center and H_2S (Cooke et al., 2014). Besides, Wilkinson et al. (2015) suggested that the chlorite Ti content is strongly related to the distance from the hydrothermal center which is consistent with thermal gradients expected around cooling intrusions, and suggested temperature of hydrothermal fluids also contribute to trace element patterns of chlorite except advective outflow of rising fluids. In addition, the protolith rocks also have influence on the chlorite and epidote compositions (Walshe, 1986; Frei et al., 2004). But for the Yandong Cu deposit, its protolith rocks are mainly basaltic to andesitic rocks in which such facts may are limited. In fact, previous studies considered chlorite and epidote compositions are sensitive to bulk rock and fluid compositions, pH, temperature, fugacities of O_2, CO_2 and S (Kranidiotis and MacLean, 1987; Frei et al., 2004; Bourdelle et al., 2013). Therefore, further studies are needed to unravel which factors are the most important for trace element patterns of chlorite and epidote in the Yandong Cu deposit.

6.2. Ore geneiss implications

Unresolved genetic issues of the Yandong Cu deposit include: (1) Age dating of the ore-bearing tonalite porphyry yielded ca. 340–332 Ma (Han et al., 2014; Shen et al., 2014a; Xiao et al., 2016), which is significantly older than the mineralization age (ca. 323 Ma; Rui et al., 2002), casting doubt on whether the tonalite porphyry was the causative porphyry. (2) Potassic alteration appears to be less developed, at least at the current exploration depth. (3) the Yandong orebody is generally platy-shaped (Han et al., 2006; Xiao et al., 2016), and 4) Fluid inclusion studies indicated that the ore-forming fluids were of very low temperature (ca. 200 °C; Han et al., 2006; Zhang et al., 2010). All these features are different from typical porphyry Cu deposits (Sillitoe, 2010.

The Yandong tonalite porphyry shows oxidized adakite geochemical affinity, and its age (ca. 340–332 Ma) is consistent with the phyllic alteration age (sericite K-Ar: 341.0 ± 4.9 Ma). However, the tonalite porphyry has lower zircon Ce^{4+}/Ce^{3+} ratios (78–728, avg. 250) and whole-rock $(La/Yb)_N$ ratios (Xiao et al., 2016) than adakitic rocks from large porphyry Cu deposits in Chile (e.g., El Teniente, Muñoz et al., 2012), indicating that the tonalite porphyry may have relatively weak porphyry Cu mineralization potential. Compared with the Yandong tonalite porphyry, the Yandong quartz porphyry shows even lower zircon Ce^{4+}/Ce^{3+} ratios (8–208, avg. 69) and no adakitic affinities (Xiao et al., 2016), and its age overlap the main mineralization age (ca. 323 Ma). These indicate that the quartz albite porphyry (granitic) may not have produced porphyry Cu mineralization but was related to the late overprinting mineralization stage, which is consistent with that the quartz albite porphyry (granitic) do not occur in the Exploration Line 16 and Cu mineralization was weak. The mineral assemblage developed in the main mineralization stage contains chalcopyrite + chlorite + anhydrite + calcite (locally coarse-grained), which overprinted the phyllic alteration in the early porphyry mineralization (Fig. 5H). This mineralization style is obviously different from porphyry Cu deposit (dominated by quartz + sulfides stockwork; Sillitoe, 2010). Unlike typical porphyry Cu deposits, potassic alteration was not well developed at Yandong and the shape of Yandong orebody is platy-like, which is also different from typical porphyry Cu deposits (Lowell and Guilbert, 1970). Therefore, the Yandong Cu deposit is not a typical porphyry deposit, although most of the Yandong Cu orebody is hosted in the tonalite porphyry. The tonalite porphyry may have been related to early porphyry Cu mineralization and introduced ore-forming materials, but the later quartz albite porphyry (granitic) may have brought another stage of hydrothermal fluid and caused overprinting Cu mineralization. Correspondingly, the chemical compositions of chlorite and epidote also suggest that both porphyry-mineralization-related and -unrelated propylitic alteration have occurred at Yandong.

Textual relationship of chlorite with chalcopyrite indicates that chlorite intergrown with chalcopyrite in this stage and chlorite represents a fluid-present phase during hydrothermal precipitation of chalcopyrite. Thus, equilibrium with the fluid at a local scale may be assumed based on the mineral chemistry of chlorite. The

chlorite thermometer of Kranidiotis and MacLean (1987) was used, which is based on the variation in tetrahedral Al content and Fe/(Fe + Mg) ratio according to the equation: T = 74.2 * Fe/(Fe + Mg) + 212 * Al^{IV} + 18. Calculated temperatures of Chl-1 show a large variation temperatures of 217 to 309 °C with an average of 267 °C, while Chl-2 show a higher temperature ranging from 249 to 384 °C with an average of 319 °C, indicating that the main Cu deposition occurred at medium–high temperatures (249–384 °C), which is obviously higher than temperature of fluid inclusions obtained in previous studies (most about 200 °C). This can be explained by that fluid inclusions in previous studies are mostly from quartz which is developed in the late stage of porphyry mineralization, but not in the overprinting stage (Han et al., 2006; Zhang et al., 2010). The Stage IV ore-forming temperature falls into the middle-high temperature hydrothermal fluid range, overlapping with that of magmatic-hydrothermal fluids (Chen and Li, 2009), which coincide with the conclusion that the overprinting mineralization was related to the quartz albite porphyry (granitic). Moreover, fluid inclusions and C-H-O-S stable isotopes also indicate that the Yandong ore fluids were mainly magma-derived (Han et al., 2006; Zhang et al., 2010). Chl-2 is Fe-rich, which is also found in other deposits associated with Cu mineralization or Au mineralization (e.g., the Thanewasna Cu-Au deposit and the Huogeqi Cu deposit, Zhong et al., 2012; Dora and Randive, 2015). It is shown that this kind of Fe-rich chlorite is related to fluid boiling under reduced conditions (Zang and Fyfe, 1995; Dora and Randive, 2015).

7. Conclusions

(1) Major alteration and mineralization at Yandong can be divided into the propylitic alteration, quartz-magnetite alteration, phyllic alteration and early mineralization, overprinting mineralization, and late vein and supergene stages.
(2) The adakitic tonalite porphyry and quartz albite porphyry (granitic) may have been causative to the early and overprinting Cu mineralization, respectively.
(3) Chlorite from the overprinting mineralization stage contains lower SiO_2, MgO, Cr, Ni, Co, B, Ca and Sr and Mn, but higher FeO, Al_2O_3, Fe/(Fe + Mg), Sc, Ga, Sn, Ti and Zn than chlorite from the propylitic alteration stage. Epidote from the overprinting mineralization stage contains lower B, Zr, Ba and Ti, but higher Sn, Y, Ga, Ag, U, Y, Cu and Sr than epidote from the early propylitic alteration stage.
(4) Titanium and V of chlorite, and Sb of epidote show similar spatial variations in the young and ancient porphyry deposits, and these patterns may be useful for exploration vectoring for Paleozoic porphyry Cu deposits.

Acknowledgements

This study was funded by the Chinese National 973-Program (2014CB440802), CAS/SAFEA International Partnership Program for Creative Research Team (20140491534) and CAS 100 Talent Program (Y333081A07). We are grateful to Li Congying for assisting with the LA–ICP–MS chlorite analysis. This is contribution No. IS-2362 from GIGCAS.

Appendix A. Supplementary data

Supplementary data associated with this article can be found, in the online version, at http://dx.doi.org/10.1016/j.oregeorev.2017.03.004.

References

Arnason, J.G., Bird, D.K., Liou, J.G., 1993. Variables controlling epidote composition in hydrothermal and low-pressure regional metamorphic rocks, Abh. Geol. B.A.
Bryndzia, L.T., Scott, S.D., 1987. The composition of chlorite as a function of sulfur and oxygen fugacity; an experimental study. Am. J. Sci. 287, 50–76.
Bourdelle, F., Parra, T., Chopin, C., Beyssac, O., 2013. A new chlorite geothermometer for diagenetic to low-grade metamorphic conditions. Contrib. Miner. Petrol. 165, 723–735.
Cameron, E.M., Leybourne, M.I., Reich, M., Palacios, C., 2010. Geochemical anomalies in northern Chile as a surface expression of the extended supergene metallogenesis of buried copper deposits. Geochem. Explor. Environ. Anal. 10, 157–169.
Carranza, E.J.M., Sadeghi, M., 2012. Primary geochemical characteristics of mineral deposits—implications for exploration. Ore Geol. Rev. 45, 1–4.
Cathelineau, M., 1988. Cation site occupancy in chlorites and illites as function of temperature. Clay Miner. 23, 471–485.
Chang, Z.S., Hedenquist, J.W., White, N.C., Cooke, D.R., Roach, M., Deyell, C.L., Garcia, J., Gemmell, J.B., McKnight, S., Cuison, A.L., 2011. Exploration tools for linked porphyry and epithermal deposits: example from the Mankayan intrusion-centered Cu-Au district, Luzon, Philippines. Econ. Geol. 106, 1365–1398.
Chen, H.Y., Yang, J.T., Baker, M., 2012. Mineralization and fluid evolution of the Jiyuan polymetallic Cu–Ag–Pb–Zn–Au deposit, eastern Tianshan, NW China. Int. Geol. Rev. 54, 816–832.
Chen, Y.J., Li, N., 2009. Nature of ore-fluids of intracontinental intrusion-related hypothermal deposits and its difference from those in island arcs. Acta Petrol. Sin. 25, 2477–2508 (in Chinese with English abstract).
Cooke, D.R., Baker, M., Hollings, P., Sweet, G., Chang, Z., Danyushevsky, L., Gilbert, S., Zhou, T., White, N.C., Gemmell, J.B., 2014. New advances in detecting the distal geochemical footprints of porphyry systems—epidote mineral chemistry as a tool for vectoring and fertility assessments. Econ. Geol. Special Publ. 18, 127–152.
Deer, W.A., Howie, R.A., Iussman, J., 1962. Rock-Forming Minerals: Sheet Silicates. Longman, London.
Dora, M.L., Randive, K.R., 2015. Chloritisation along the Thanewasna shear zone, Western Bastar Craton, Central India: Its genetic linkage to Cu–Au mineralisation. Ore Geol. Rev. 70, 151–172.
Foster, M.D., 1962. Interpretation of the Composition and a Classification of the Chlorites. The United States Geological Survey. Professional Paper.
Frei, D., Liebscher, A., Franz, G., Dulski, P., 2004. Trace element geochemistry of epidote minerals. Rev. Mineral. Geochem. 56, 553–605.
Han, C.M., Xiao, W.J., Zhao, G.C., Mao, J.W., Yang, J.M., Wang, Z.L., Yan, Z., Mao, Q.G., 2006. Geological characteristics and genesis of the Tuwu porphyry copper deposit, Hami, Xinjiang, Central Asia. Ore Geol. Rev. 29, 77–94.
Han, Z.K., Han, C.M., Xiao, W.J., Zhao, G.C., Wang, Z.M., Ao, S.J., Zhang, J., Wan, B., 2014. Palaeozoic porphyry Cu–Au and ultramafic Cu–Ni deposits in the eastern Tianshan orogenic belt: temporal constraints from U-Pb geochronology. Int. Geol. Rev. 55, 842–862.
Hou, T., Zhang, Z.C., Santosh, M., Encarnacion, J., Zhu, J., Luo, W.J., 2014. Geochronology and geochemistry of submarine volcanic rocks in the Yamansu iron deposit, Eastern Tianshan Mountains, NW China: Constraints on the metallogenesis. Ore Geol. Rev. 56, 487–502.
Inoue, A., Kurokawa, K., Hatta, T., 2010. Application of chlorite geothermometry to hydrothermal alteration in toyoha geothermal system, southwestern Hokkaido, Japan. Resour. Geol. 60, 52–70.
Jago, C.P., Tosdal, R.M., Cooke, D.R., Harris, A.C., 2014. Vertical and lateral variation of mineralogy and chemistry in the early Jurassic Mt. Milligan alkalic porphyry Au-Cu deposit, British Columbia, Canada. Econ. Geol. 109, 1005–1033.
Kranidiotis, P., MacLean, W.H., 1987. Systematics of chlorite alteration at the Phelps Dodge massive sulfide deposit, Matagami, Quebec. Econ. Geol. 82, 1898–1911.
Li, Z.M., Zhao, R.F., Huo, R.P., Wang, Q.M., 2006. Geological characters of Tuwu-Yandong copper deposits in Xinjiang. Geol. Prospect. 42, 1–4 (in Chinese with English abstract).
Li, D.F., Chen, H.Y., Zhang, L., Hollings, P., Chen, Y.J., Lu, W.J., Zheng, Y., Wang, C.M., Fang, J., Chen, G., Zhou, G., 2016. Ore geology and fluid evolution of the giant Caixiashan carbonate-hosted Zn–Pb deposit in the Eastern Tianshan, NW China. Ore Geol. Rev. 1, 355–372.
Lowell, J.D., Guilbert, J.M., 1970. Lateral and vertical alteration-mineralization zoning in porphyry ore deposits. Econ. Geol. 65, 373–408.
Liu, Y.S., Hu, Z.C., Gao, S., Günther, D., Xu, J., Gao, C.G., Chen, H.H., 2008. In situ analysis of major and trace elements of anhydrous minerals by LA-ICP-MS without applying an internal standard. Chem. Geol. 257, 34–43.
Lu, L., Zhu, L.X., Xiao, K.Y., Ma, S.M., Yin, J.N., Xu, M.Z., 2012. Geochemical features and metallogenic prediction of the Caixiashan-Weiquan area in the East Tianshan region. Acta Geol. Sinica-English Edition 86, 885–893.
Mao, J.W., Pirajno, F., Zhang, Z.H., Chai, F.M., Wu, H., Chen, S.P., Cheng, L.S., Yang, J.M., Zhang, C.Q., 2008. A review of the Cu–Ni sulphide deposits in the Chinese Tianshan and Altay orogens (Xinjiang Autonomous Region, NW China): Principal characteristics and ore-forming processes. J. Asian Earth Sci. 32, 184–203.
Mao, Q.G., Xiao, W.J., Fang, T.H., Windley, B.F., Sun, M., Ao, S.J., Zhang, J.E., Huang, X.K., 2014. Geochronology, geochemistry and petrogenesis of Early Permian alkaline magmatism in the Eastern Tianshan: implications for tectonics of the Southern Altaids. Lithos 190–191, 37–51.
Monteiro, L.V.S., Xavier, R.P., Hitzman, M.W., Juliani, C., de Souza Filho, C.R., Carvalho, E.d.R., 2008. Mineral chemistry of ore and hydrothermal alteration at

the Sossego iron oxide–copper–gold deposit, Carajás Mineral Province, Brazil. Ore Geol. Rev. 34, 317–336.
Muñoz, M., Charrier, R., Fanning, C., Maksaev, V., Deckart, K., 2012. Zircon trace element and O-Hf Isotope analyses of mineralized intrusions from El Teniente ore deposit, Chilean Andes: constraints on the source and magmatic evolution of porphyry Cu–Mo related magmas. J. Petrol. 53, 1091–1122.
No.1 geological party Xinjiang Bureau of Geology and Mineral exploration, 2012. The Exploration Report of Tuwu Copper Deposit. Hami, Xinjiang.
Perelló, J., Cox, D., Garamjav, D., Sanjdorj, S., Diakov, S., Schissel, D., Munkhbat, T.O., Oyun, G., Tolgoi, Oyu, 2001. Mongolia: Siluro-Devonian Porphyry Cu-Au-(Mo) and High-Sulfidation Cu Mineralization with a Cretaceous Chalcocite Blanket. Econ. Geol. 96, 1407–1428.
Qin, K.Z., Sun, S., Li, J.L., Fang, T.H., Wang, S.L., Liu, W., 2002. Paleozoic epithermal Au and porphyry Cu deposits in north Xinjiang, China: epochs, features, tectonic linkage and exploration significance. Resour. Geol. 52, 291–300.
Rui, Z.Y., Wang, L.S., Wang, Y.T., Liu, Y.L., 2002. Discussion on metallogenic epoch of Tuwu and Yandong porphyry copper deposits in eastern Tianshan Mountains, Xinjiang. Mineral Deposit 21, 16–22 (in Chinese with English abstract).
Shen, P., Pan, H.D., Dong, L.H., 2014a. Yandong porphyry Cu deposit, Xinjiang, China—Geology, geochemistry and SIMS U-Pb zircon geochronology of host porphyries and associated alteration and mineralization. J. Asian Earth Sci. 80, 197–217.
Shen, P., Pan, H.D., Zhou, T.F., Wang, J.B., 2014b. Petrography, geochemistry and geochronology of the host porphyries and associated alteration at the Tuwu Cu deposit, NW China: a case for increased depositional efficiency by reaction with mafic hostrock? Miner. Deposita 49, 709–731.
Sillitoe, R.H., 2010. Porphyry copper systems. Econ. Geol. 105, 3–41.
Watanabe, Y., Stein, H.J., 2000. Re-Os ages for the Erdenet and Tsagaan Suvarga porphyry Cu-Mo deposits, Mongolia, and tectonic implications. Econ. Geol. 95, 1537–1542.
Wang, Y.H., Xue, C.J., Wang, J.P., Peng, R.M., Yang, J.T., Zhang, F.F., Zhao, Z.N., Zhao, Y. J., 2015. Petrogenesis of magmatism in the Yandong region of Eastern Tianshan, Xinjiang: geochemical, geochronological, and Hf isotope constraints. Int. Geol. Rev. 57, 1130–1151.
Wang, Y.F., Chen, H.Y., Xiao, B., Han, J.S., Yang, J.T., 2016. Prophyritic-overlapped mineralization of Tuwu and Yandong copper deposits in Eastern Tianshan Mountains, Xinjiang. Mineral Deposits 35, 51–68 (in Chinese with English abstract).
Wilkinson, J.J., Chang, Z.S., Cooke, D.R., Baker, M.J., Wilkinson, C.C., Inglis, S., Chen, H. Y., Bruce Gemmell, J., 2015. The chlorite proximitor: a new tool for detecting porphyry ore deposits. J. Geochem. Explor. 152, 10–26.
Walshe, J.L., 1986. A six-component chlorite solid solution model and the conditions of chlorite formation in hydrothermal and geothermal systems. Econ. Geol. 81, 681–703.
Wu, C., Chen, H.Y., Hollings, P., Xu, D.R., Liang, P., Han, J.S., Xiao, B., Cai, K.D., Liu, Z.J., Qi, Y.K., 2015. Magmatic sequences in the Halasu Cu Belt, NW China: Trigger for the Paleozoic porphyry Cu mineralization in the Chinese Altay-East Junggar. Ore Geol. Rev. 71, 373–404.
Wu, H., Li, H.Q., Chen, F.W., Lu, Y.F., Deng, G., Mei, Y.P., Ji, H.G., 2006. Zircon SHRIMP U-Pb dating of plagiogranite porphyry in the Chihu molybdenum-copper district, Hami, East Tianshan. Geol. Bull. Chin. 25, 549–552 (in Chinese with English abstract).
Xiao, B., Chen, H.Y., Hollings, P., Han, J.S., Wang, Y.F., Yang, J.T., Cai, K.D., 2016. Magmatic evolution of the Tuwu-Yandong porphyry Cu belt, NW China: Constraints from geochronology, geochemistry and Sr–Nd–Hf isotopes. Gondwana Res. http://dx.doi.org/10.1016/j.gr.2015.1009.1003.
Xiao, W.J., Windley, B.F., Huang, B.C., Han, C.M., Yuan, C., Chen, H.L., Sun, M., Sun, S., Li, J.L., 2009. End-Permian to Mid-Triassic termination of the accretionary processes of the southern Altaids: implications for the geodynamic evolution, Phanerozoic continental growth, and metallogeny of Central Asia. Int. J. Earth Sci. 98, 1189–1217.
Xiao, W.J., Zhang, L.C., Qin, K.Z., Sun, S., Li, J.L., 2004. Paleozoic accretionary and collisional tectonics of the eastern Tianshan (China): implications for the continental growth of central Asia. Am. J. Sci. 304, 370–395.
Yang, F.Q., Mao, J.W., Pirajno, F., Yan, S.H., Liu, G.R., Zhou, G., Zhang, Z.X., Liu, F., Geng, X.X., Guo, C.L., 2012. A review of the geological characteristics and geodynamic setting of Late Paleozoic porphyry copper deposits in the Junggar region, Xinjiang Uygur Autonomous Region, Northwest China. J. Asian Earth Sci. 49, 80–98.
Zang, W., Fyfe, W.S., 1995. Chloritization of the hydrothermally altered bedrock at the Igarapé Bahia gold deposit, Carajás, Brazil. Miner. Deposita 30, 30–38.
Zhang, D.Y., Zhou, T.F., Yuan, F., Fan, Y., Liu, S., Peng, M.X., 2010. Geochemical characters, metallogenic chronology and geological significance of the Yanxi copper deposit in eastern Tianshan, Xinjiang. Acta Petrologica Sinica 26, 3327–3338 (in Chinese with English abstract).
Zhang, L.C., Qin, K.Z., Xiao, W.J., 2008. Multiple mineralization events in the eastern Tianshan district, NW China: isotopic geochronology and geological significance. J. Asian Earth Sci. 32, 236–246.
Zhang, L.C., Xiao, W.J., Qin, K.Z., Zhang, Q., 2006. The adakite connection of the Tuwu-Yandong copper porphyry belt, eastern Tianshan, NW China: trace element and Sr-Nd-Pb isotope geochemistry. Miner. Deposita 41, 188–200.
Zhang, W.F., Chen, H.Y., Han, J.S., Zhao, L.D., Huang, J.H., Yang, J.T., Yan, X.L., 2015. Geochronology and Geochemistry of Igneous Rocks in the Bailingshan Area: Implications for the Tectonic Setting of Late Paleozoic Magmatism and Iron Skarn Mineralization in the Eastern Tianshan. Gondwana Research, NW China. 10.1016/j.gr.2015.1010.1011.
Zhong, R.C., Li, W.B., Chen, Y.J., Huo, H.L., 2012. Ore-forming conditions and genesis of the Huogeqi Cu–Pb–Zn–Fe deposit in the northern margin of the North China Craton: Evidence from ore petrologic characteristics. Ore Geol. Rev. 44, 107–120.